JOURNAL OF APPLIED ELECTROCHEMISTRY 25 (1995) 340–346

Copper removal from aerated solution containing various metal ions using an undivided rotating cylinder electrode reactor

N. MASSÉ, J. ST-PIERRE, M. BERGERON

INRS-Géoressources, 2700 Rue Einstein, Case Postale 7500, Ste-Foy, Québec, Canada, G1V 4C7

Received 26 April 1994; revised 24 September 1994

Potentiostatic control of a rotating cylinder electrode reactor enabled copper retrieval from a solution containing multiple metallic ions. The treated solution (pH 4 sulphuric acid) was obtained from a mine tailing. A batch process was used in laboratory experiments to simulate possible industrial treatments. Oxygen reduction was the major parasitic reaction at the cylinder cathode since the reactor was not separated, allowing the gas produced at the anode to dissolve in the electrolyte. A higher current therefore generated an increase in oxygen production and an increase in dissolved oxygen concentration. Since the oxygen reduction proceeded under diffusion control, the oxygen reduction current efficiency also increased. Reduction of ferric ions to a ferrous state and arsenic deposition were other less important side reactions decreasing current efficiency. Polarization experiments were conducted using a rotating disk electrode to study the reactions encountered at the cylinder cathode.

List of symbols

a	constant used in Equation 3
A	cathode active surface (cm^2)
c	concentration ($mol\,cm^{-3}$)
d	diameter (cm)
D	diffusion coefficient ($cm^2\,s^{-1}$)
F	Faraday constant ($96\,490\,C\,mol^{-1}$)
H	cylinder height (cm)
I	current (A)
k	mass transfer coefficient ($cm\,s^{-1}$)
n	number of electrons exchanged in the global reaction
Re	Reynolds number ($\omega d^2/2\nu$)
Sc	Schmidt number (ν/D)
Sh	Sherwood number (kd/D)
t	time (s)
V	solution volume (cm^3)

Greek symbols

ν	kinematic viscosity ($cm^2\,s^{-1}$)
ω	angular speed ($rad\,s^{-1}$)

Subscripts

c	cylinder
Cu	copper
d	disc
Fe	iron
l	limiting
t	at time t
0	initial

1. Introduction

Ore processing in mineral dressing plants produces large quantities of residue which are deposited in tailing ponds [1]. Sulphide oxidation taking place in tailings leads to the formation of metal-rich acidic water. Important environmental hazards are associated with the dispersion of these fluids in the surrounding ecosystems [2, 3]. A barrier limiting water and/or oxygen access to sulphides is a possible abatement measure. Barrier technology is, however, very costly [4].

For the past two years, an alternative has been studied [5–7]. The main goal was to recover metals of economic interest from sulphide containing residues and in parallel, to incorporate into the treatment flowsheet procedures allowing secure deposition of the remainder. The process was based on the separation of sulphides present in tailings by flotation [7]. Sulphides are enveloped by secondary sulphates produced as a result of their oxidation. These sulphates created recovery problems at the flotation step. It was necessary to wash the flotation feed in a pH 2 sulphuric acid solution to optimize recovery. The resulting solution was enriched with dissolved metals. Electrochemical methods were developed to recover economically interesting dissolved metals from this solution.

The present paper deals with copper recovery from a solution containing dissolved oxygen and several metallic ions using a rotating cylinder electrode (RCE). Copper retrieval was identified as an essential preliminary step before zinc recuperation. The latter step will be the subject of a forthcoming paper [8].

0021-891X

Theoretical approaches and practical results are combined to predict possible problems during an operation of larger scale. The experimental solution was generated from a sulphide tailing making results applicable to a real situation.

2. Experimental details

All experiments were conducted at room temperature ($22 \pm 0.5°$ C) and at normal atmospheric pressure.

2.1. *Solution*

The solution used in the experiments was obtained from the washing step made prior to flotation of the Manitou mining residue located at Val d'Or, Québec, Canada. The solution, mostly sulphuric acid at pH 2, was first analysed by ICP–MS to identify the major elements and, secondly, by atomic absorption for more accurate determination of Fe, Zn, As, Cu, Cd and Co concentrations. Atomic absorption measurements were subject to an error of ±10%. Detection limits were lower than 1 ppm for all elements analyzed. Dissolved iron had to be removed prior to copper electrodeposition. Ferrous iron oxidation to ferric state was performed with hydrogen peroxide (H_2O_2 30%). Iron hydroxide selective precipitation was achieved by increasing pH to 4 with sodium hydroxide (4 M NaOH solution made with reagent grade chemicals and deionized water). The resulting solution, thus diluted by a factor of 1.2, was analysed by atomic absorption for Fe, Zn, As, Cu, Cd and Co.

2.2. *Polarization experiments*

Polarization experiments were performed to characterize cathodic reactions encountered with such a complex solution. A rotating disc electrode at 104.7 rad s^{-1} (1000 rpm) was used. A platinum disk with a 0.196 cm^2 surface area imbedded in a polytetrafluoroethylene cylinder was coupled to a Pine Instruments rotating disk electrode system (model AFMSRX). Platinum foil served as the insoluble anode so as to avoid contamination of the solution. The presence of anodically produced oxygen in the catholyte was reduced by separating the anodic and cathodic compartments with fritted glass. In addition, the catholyte was degassed with nitrogen overnight and during experiments. A saturated calomel electrode (SCE) and a Luggin capillary were used to eliminate the ohmic drop. Experiments were carried out with a Schlumberger 1286 electrochemical interface controlled via a PC microcomputer using the Corrware software. Polarization curves were obtained using cathodic and anodic sweeps at 5 mV s^{-1}.

2.3. *Measurement of kinematic viscosity*

Kinematic viscosity was measured with a calibrated Cannon–Fenske routine viscometer (number 25). A thermostatic Neslab bath (model RTE-100) ensured constant temperature during measurements. The viscometer was immersed for at least 10 min before each measurement. The kinematic viscosity was measured with a precision of ±0.000 02 cm^2 s^{-1}.

2.4. *Measurement of diffusion coefficient*

The solution, instrument arrangement, reference electrode and electrical setup were similar to those used in polarization experiments. The rotational speed was varied from 10.47 to 167.6 rad s^{-1} (100 to 1600 rpm) to determine the limiting current variation of copper deposition. Cathodic and anodic potential sweeps between 0 and −0.6 V vs SCE were used to estimate current values in the diffusion controlled region and were corrected for ferric ion reduction as explained in Section 3.4.

2.5. *Experimental setup using a rotating cylinder electrode reactor*

The rotating cylinder electrode reactor (RCER) consisted of an aluminium cylinder installed on a rotator (described in Section 2.2). The aluminium electrode was mounted between two polytetrafluoroethylene discs (each 1.27 cm long by 5.08 cm diam.) to eliminate edge effects. The exposed aluminium surface was 20.3 cm^2 (also 1.27 cm long by 5.08 cm diam.). The anode was constructed from a lead foil previously preconditioned by overnight dipping in 1 M sulphuric acid to favour formation of a passive layer. Lead contamination was not encountered during the experiments. At least 60 ml of solution were needed per experiment to keep the cathode properly immersed. A maximum of 100 ml could be treated with such a setup. The electrolyte was not separated and the solution was exposed to air. The interelectrode gap was 0.5 ± 0.1 cm.

The remainder of the instrument arrangement, solution, reference electrode and electrical setup were similar to those used for polarization experiments (Section 2.2). The potential was held between −0.4 and −0.7 V vs SCE to ensure diffusion controlled copper electrodeposition. Rotational speeds varying from 31.41 to 188.5 rad s^{-1} (300 to 1800 rpm) were used.

3. Results

3.1. *Chemical analysis*

Chemical analysis of the solution as received from the mining operation and after iron precipitation is given in Table 1. The precipitation step removed most of the iron and arsenic (99.99% and 97%, respectively). Copper, cadmium and cobalt were partly removed (27%, 23% and 48%, respectively) while zinc was not affected. The lower zinc concentration value in the pH 4 solution was due to dilution occurring during the precipitation treatment.

Table 1. Concentration of metallic elements in the washing solution before and after iron precipitation with corresponding reversible potentials

Metallic elements	*Concentration*/ppm		*Reversible potential/V vs SCE at 25° C after iron precipitation*
	Solution at pH 2 before iron precipitation	*Solution at pH 4 after iron precipitation*	
Fe	17000	2.3	−0.819
Zn	4400	3800	−1.040
As	150	3	−0.316
Cu	90	55	+0.009
Cd	25	16	−0.759
Co	20	8.7	−0.635

3.2. *Kinematic viscosity*

Kinematic viscosity of the pH 4 solution kept at 22° C is $0.0111\,cm^2\,s^{-1}$. Water at this temperature has a kinematic viscosity of $0.009\,58\,cm^2\,s^{-1}$ [9].

3.3. *RDE polarization experiments*

Polarization curves are shown in Fig. 1. The arrows show the potential sweep direction. The cathodic sweep initially shows a current drop associated with Fe^{2+} oxidation. This reaction is reversed at the Fe^{3+}/Fe^{2+} rest potential of about 550 mV vs SCE. At 250 mV vs SCE, the current reaches a constant value of 13 μA which corresponds to the diffusion limited Fe^{3+} reduction to Fe^{2+}. Around −50 mV vs SCE, the current increase is attributed to copper reduction (Table 1). At lower potentials of about −350 mV vs SCE, the diffusion limited copper deposition current of 145 μA is reached. This value represents the difference between the total current of 158 μA less the 13 μA needed for Fe^{3+} reduction. From the copper ion diffusion coefficient obtained in the following Section ($5.6 \times 10^{-6}\,cm^2\,s^{-1}$), Equation 2 (viscosity of $0.0111\,cm^2\,s^{-1}$, rotational speed of $104.7\,rad\,s^{-1}$ (1000 rpm)), and with the limiting currents (13 and 145 μA) and copper concentration of 55 ppm ($8.66 \times 10^{-7}\,mol\,cm^{-3}$), the calculated limiting current is 139 μA.

The anodic sweep gives approximately the same total limiting current (158 μA). Since copper deposited on the platinum disk during the cathodic sweep, copper oxidation induced a current inversion when the potential reached the Cu^{2+}/Cu reversible value.

3.4. *Copper ion diffusion coefficient*

The copper ion diffusion coefficient was derived from the Levich equation using data acquired from the RDE setup. The total current at the RDE, for potentials below −350 mV vs SCE, is the sum of the limiting current for copper and iron:

$$I_{l,d} = I_{l,Cu} + I_{l,Fe} \tag{1}$$

Equation 1 is rearranged as,

$$I_{l,d} = 0.62 n_{Cu} F A_d D_{Cu}^{2/3} \nu^{-1/6} \omega_d^{1/2} c_{Cu,0} \left(1 + \frac{I_{l,Fe}}{I_{l,Cu}}\right) \tag{2}$$

where the total current at the disc electrode is equivalent to the limiting current for copper alone, with addition of a corrective term. This correction was easily evaluated using the iron and copper limiting current ratio of 0.0897 (13 μA over 145 μA) obtained from the polarization curve data in Fig. 1. Limiting current values were obtained at 22° C for different angular velocities (Fig. 2). The slope was $1.45 \times 10^{-5}\,A\,s^{1/2}\,rad^{-1/2}$ which is equal to $I_{l,d}$ divided by $\omega_d^{1/2}$ in Equation 2. In the latter expression, only D_{Cu} was unknown, but easily determined to be $5.6 \times 10^{-6}\,cm^2\,s^{-1}$. A value of $7.3 \times 10^{-6}\,cm^2\,s^{-1}$ was

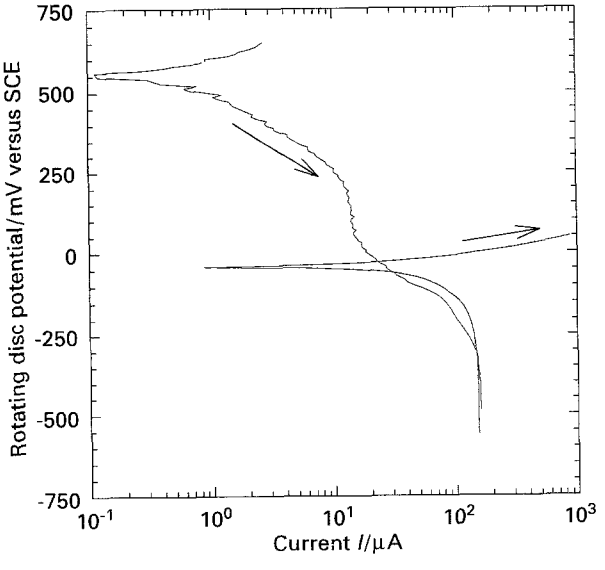

Fig. 1. Polarization curves obtained with a rotating disk electrode turning at $104.7\,rad\,s^{-1}$ (1000 rpm). The arrows show the potential sweep direction ($5\,mV\,s^{-1}$). $T = 22°$ C.

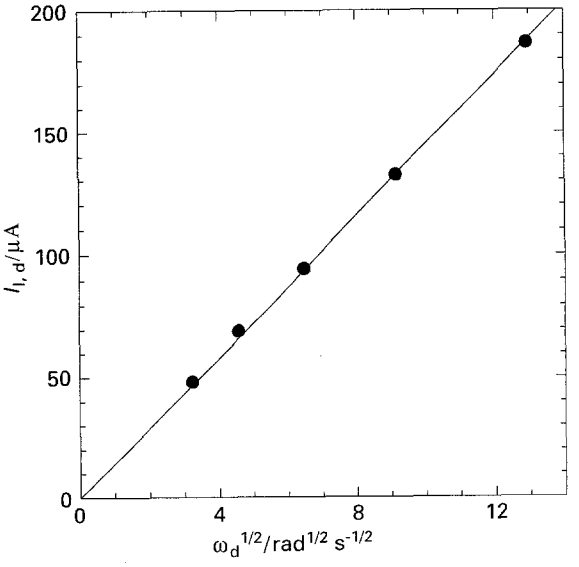

Fig. 2. Total limiting current as a function of rotational speed. The slope is equal to $1.45 \times 10^{-5}\,A\,s^{1/2}\,rad^{-1/2}$ and $D_{Cu} = 5.6 \times 10^{-6}\,cm^2\,s^{-1}$. $T = 22°$ C.

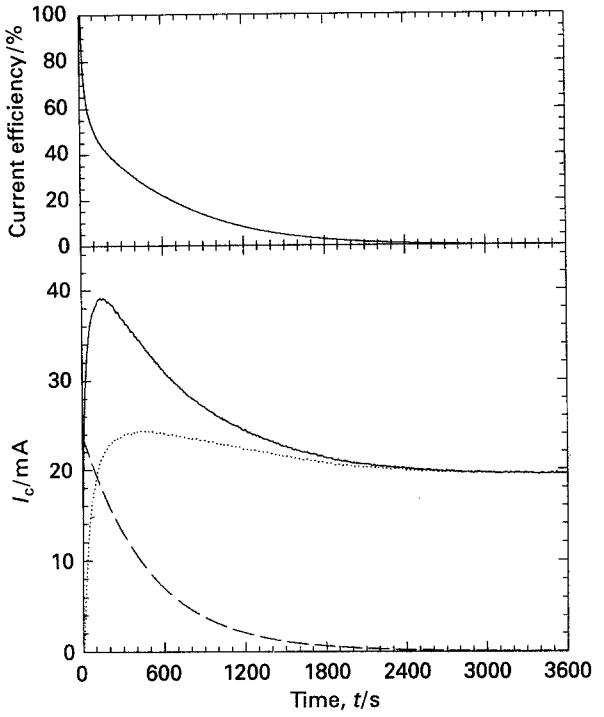

Fig. 3. Potentiostatic experiment results (−0.6 V vs SCE) using a rotating cylinder electrode turning at 188.5 rad s^{-1} (1800 rpm, $V = 70$ ml). Bottom: the full line represents total current, the dashed line corresponds to the theoretical copper deposition current and the dotted line represents the difference between these two currents. Top: theoretical current efficiency.

reported in the literature for a similar solution and temperature [10].

3.5. *RCE potentiostatic experiments*

Representative potentiostatic results are illustrated in Fig. 3. The full line in the figure (bottom part) shows current evolution. For the first 120 seconds, the current increases from zero to 39 mA. Afterwards, the current decreases to 19.5 mA (at 3000 s) and remains constant thereafter.

Copper concentration after iron precipitation was 55 ppm (Table 1). Afterwards, the RCER, operated under the particular experimental conditions of Figure 3, led to a reduction in copper concentration to 1.7 ppm after 2000 s. This value will be compared to the theoretical concentration.

4. Discussion

4.1. *Copper retrieval with a RCER*

Initially, the potentiostatic separation of metals using a RCER was considered for analytical purposes [11]. It was subsequently studied for industrial applications such as electrolyte purification or metal recovery for Ni plating (Cu, Fe and Zn removal) [12], Zn electrowinning (Cd removal) [13] and various plating or industrial effluents [14, 15]. These studies have shown that a selective separation is possible for the most noble metal in the solution [14], although copper removal from the liquid produced during mine residue treatment has not been previously studied.

The reversible potential of metals present in the electrolyte at 25° C are given in Table 1. Although iron does not deposit in the potential range investigated for copper deposition (−0.4 to −0.7 V vs SCE), this impurity creates a loss of current efficiency. Cadmium and zinc cannot deposit in this range and therefore cannot contaminate the copper deposit. However, the purity may be somewhat decreased by arsenic and, to a lesser extent, by cobalt, since a limiting current is probably not reached. In the latter case, contamination is easily avoided by using nobler potential values than the lower range limit of −0.7 V vs SCE used here.

RCER mass transfer behaviour is well documented in the literature [16–19]. The semi-empirical correlation for species diffusion to a rotating cylinder in turbulent flow is given by the equation:

$$Sh = 0.079\, Re^{a} Sc^{0.356} \tag{3}$$

where a is equal to 0.7 or 0.92 depending on whether the cylinder surface is smooth or rough, respectively. The turbulent flow occurs when Re is greater than 200. Since the smallest value of Re for all the RCER experiments was equal to 12 000, turbulence was always present.

The amount of copper deposited was insufficient to cause the formation of a rough surface. A typical roughness is 0.02 cm [17] while the maximum copper deposit thickness obtained here was 0.000 03 cm (copper dissolved in 100 ml at a concentration of 55 ppm and deposited on a 20 cm^2 surface). Therefore, a was taken to be 0.7.

The limiting current at a cylinder electrode is

$$I_{l,c} = nFkA_c c_{Cu,t} \tag{4}$$

where kA_c is obtained by expanding Equation 3:

$$kA_c = 0.079\pi(2^{-0.7})\, Hd^{1.4} D_{Cu}^{0.644} \nu^{-0.344} \omega_c^{0.7} \tag{5}$$

In the case of diffusion controlled copper deposition in batches [16–19], the change in copper concentration is expected to obey the following equation:

$$\frac{c_{Cu,t}}{c_{Cu,0}} = e^{-kA_c t/V} \tag{6}$$

The theoretical copper concentration value derived from Equations 5 and 6 using experimental conditions ($c_{Cu,0} = 55$ ppm, $V = 70$ ml, $\omega_c = 188.5$ rad s^{-1} (1800 rpm)) was 0.93 ppm at $t = 2000$ s. This resembles the measured value of 1.7 ppm. Equation 6 can therefore be used to predict the copper concentration in a complex solution.

Equation 4 can also be used to predict the copper deposition limiting current. Near a copper concentration of 1 ppm, the current is expected to be lower than 0.8 mA. The difference between this current and the measured value of approximately 20 mA (Fig. 3) is due to parasitic reactions at the cathode. The solution contains iron and, as demonstrated in

Fig. 1, can be reduced at the cathode (Equation 8). The solution was exposed to air, which resulted in an oxygen reduction side reaction current (Equation 7). Finally, as the reactor was not separated, reverse reactions given by Equations 7 and 8 took place at the anode and, consequently, regenerated O_2 and Fe^{3+} in the solution.

$$O_2 + 4H^+ + 4e^- \longrightarrow 2H_2O \quad (7)$$

$$Fe^{3+} + e^- \longrightarrow Fe^{2+} \quad (8)$$

The current due to the parasitic reaction of Fe^{3+} reduction at the RCE was estimated based on results in Fig. 1, obtained using a RDE with the limiting current following Equation 2. Since the same solution was used in both the RDE and RCE experiments, by combining Equations 2 (with $c_{Cu,0} = 0$), 4 and 5 the following relationship is obtained:

$$I_{l,c} = \frac{0.25 I_{l,d} H d^{1.4} \omega_c^{0.7}}{A_d D_{Fe}^{0.023} \nu^{0.177} \omega_d^{0.5}} \quad (9)$$

The value of ω_d in Fig. 1 was 104.7 rad s^{-1} (1000 rpm) and $A_d = 0.196\,cm^2$ while $\nu = 0.0111\,cm^2\,s^{-1}$, $H = 1.27$ cm and $d = 5.08$ cm. The iron diffusion coefficient was not measured for the present solution but the exponent of D_{Fe} in Equation 9 was low (0.023). Therefore, the value of D_{Fe} taken as $10 \times 10^{-6}\,cm^2\,s^{-1}$, has very little effect on $I_{l,c}$.

The iron limiting current in Fig. 1 was 13 μA and at rotation speeds of 31.41, 62.83, 167.6 and 188.5 rad s^{-1}(300, 600, 1600 and 1800 rpm), calculated $I_{l,c}$ values were 0.6, 1, 2 and 2.3 mA, respectively. These current values are an estimate of the side reaction current due to Fe^{3+} reduction and represent approximately 10% of the current associated to parasitic reactions. The remainder of this current is caused by oxygen reduction.

The theoretical copper reduction current was calculated (Fig. 3, dashed line) to estimate the current associated to parasitic reactions. The value of kA_c in Equation 5 was constant during the experiments. The left hand side of Equation 6 (copper concentration at time t to initial copper concentration ratio) is then equal to the limiting current ratio at time t and zero (Equation 4). The current for a diffusion controlled reaction obtained by rearranging Equations 4, 5 and 6 is

$$I_{l,c} = nFkA_c c_{Cu,0}\, e^{-kA_c t/V} \quad (10)$$

The dotted line in Fig. 3 represents the difference between experimental and theoretical results. The curves representing the current associated to parasitic reactions and total current are similar in shape. It seems therefore, that the oxygen reduction current, representing approximately 90% of the current associated to parasitic reactions, was not constant during the experiments. Consequently, since oxygen reduction proceeded at its limiting value, dissolved oxygen concentration in the cell varied during the experiments. From a qualitative point of view, dissolved oxygen concentration was influenced by the total current because it directly affected the amount of oxygen produced at the anode.

The current efficiency for copper electrodeposition was altered by side reactions. The copper current efficiency is defined as the copper current to total current ratio, and is illustrated in the upper part of Fig. 3 by using data from the bottom part of the same figure. Current efficiency was high at the beginning of the potentiostatic experiments because oxygen and iron reduction rates were small. As total current increased, the fraction pertaining to oxygen reduction also increased. The net result was a dramatic loss of current efficiency for the first 120 s. Afterwards, as copper concentration decreased, copper deposition current also diminished, while the oxygen and iron reduction currents remained almost constant. Consequently, the copper deposition current efficiency decreased. After 3000 s, the current efficiency was considered zero and all the current was used for oxygen and iron reduction.

As the copper concentration decreased, the oxygen reduction current increased. This factor should be taken into consideration in the flow sheet of an industrial plant. Since solution degassing prior to its introduction in the RCER incurs additional costs to an industrial process, the system should be optimized for high current efficiency. The study of the variables affecting dissolved oxygen concentration inside a RCER will help optimize operating conditions.

4.2. *Effect of dissolved oxygen*

The effect of oxygen at various metal RCEs was studied previously with an emphasis on corrosion behaviour [20, 21]. Consequently, these studies are of little use here since data on dissolved oxygen concentration and mechanisms affecting it are not discussed. Figure 4 illustrates the different mechanisms by which the dissolved oxygen concentration is modified in an unsealed and undivided RCER operating under batch conditions. At the cathode, some dissolved oxygen reacts. In the electrolyte bulk, the generated bubbles and atmosphere contribute to the partial desorption or absorption of dissolved oxygen. At the anode, oxygen production takes place producing both bubbles and dissolved gas.

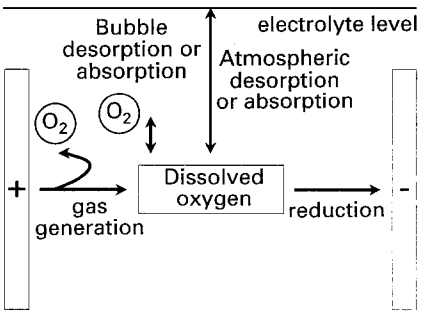

Fig. 4. Diagram showing the different mechanisms by which the dissolved oxygen concentration is modified in an unsealed and undivided RCER operating under batch conditions. Arrows represent dissolved oxygen fluxes.

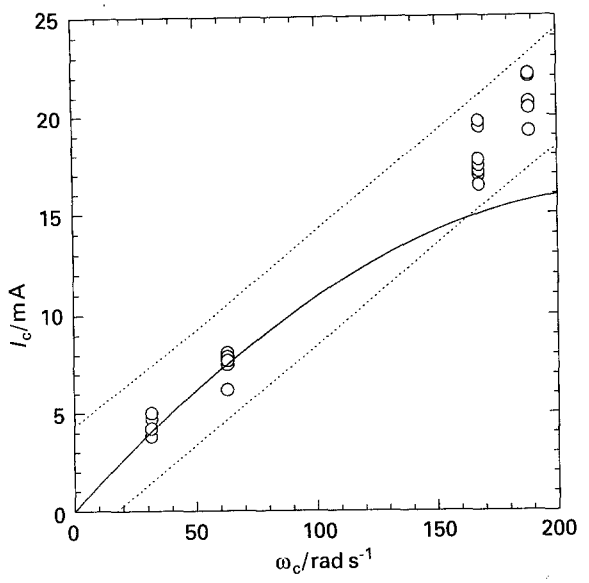

Fig. 5. Steady state oxygen reduction current as a function of rotational speed. The dotted line represents the 99% prediction interval. The full line corresponds to the theoretically predicted oxygen reduction current proportional to $\omega^{0.7}$.

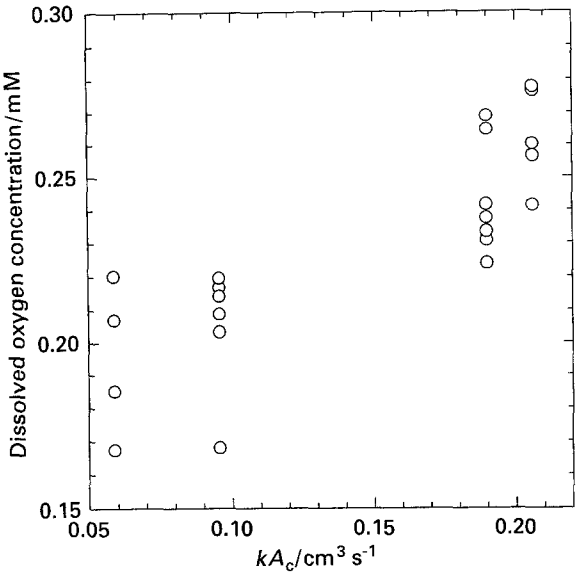

Fig. 6. Dissolved oxygen concentrations as a function of the mass transfer coefficient and electrode active surface product. The oxygen diffusion coefficient was equal to 1×10^{-5} cm^2 s^{-1}.

Current values measured at the end of each potentiostatic experiment (a constant value after 3000 s as shown in Fig. 3) were used to study the oxygen reaction behaviour (approximately 10% of these values result from the effect of Fe^{3+} reduction, see preceding Section). Statistical analysis of the cylinder rotation effect was performed with these values. The results are summarized in Fig. 5. The dotted lines indicate the 99% prediction interval. Experimental results did not follow the theoretical prediction, as explained below.

The cathodic potentials maintained during potentiostatic experiments were in the range where oxygen reduction is diffusion controlled. Equations 4 and 5 then describe the oxygen reduction current behaviour. The oxygen limiting current is then proportional to $\omega^{0.7}$ (Equation 5). This relationship is shown by the full line in Fig. 3. At low rotation speeds (less than 100 rad s^{-1}), the full line lies within the prediction interval. At higher rotation speeds, it falls outside the interval. Therefore, at higher rotation speeds, there is a factor other than ω, which increases the oxygen reduction limiting current.

The only other variable parameter in Equations 4 and 5, besides ω, is the dissolved oxygen concentration. Three sources of oxygen were identified: air, oxygen bubbles and oxygen production (Fig. 4). The latter is influenced by the cell current. Since rotation speed directly influences the total current, it indirectly affects oxygen evolution and thus the dissolved gas concentration as well, until a quasi-equilibrium is reached.

Rotation speed modifies dissolved copper and oxygen mass transport simultaneously and, hence, the total current. However, other mechanisms control the dissolved oxygen concentration and therefore a different mass transport dependency is exhibited. Although Equation 5 is valid at low rotation speeds (I_l proportional to $\omega^{0.7}$), at higher values the dissolved oxygen reduction current is proportional to ω.

An understanding of the relationship between each parameter involved in reactor design helps optimize industrial operational conditions. Extensive analysis of dissolved oxygen behaviour has been presented in other papers [22, 23] since its parasitic reaction can greatly affect copper electrodeposition current efficiency at low concentrations.

For example, if the oxygen diffusion coefficient is 10^{-5} cm^2 s^{-1}, Equations 4 and 5 allow computation of dissolved oxygen concentrations and mass transfer coefficients. These are plotted in Fig. 6 and show some scatter. At the beginning of each experiment, since dissolved oxygen concentration was not standardized and an unsteady state was studied, the results were sensitive to the initial conditions prevailing in the reactor. The concentrations obtained were within the expected range, considering that the atmospheric oxygen content is approximately 20% and that oxygen solubility is approximately 1 mM [22]. It is highly plausible that atmospheric desorption is the predominant mechanism affecting dissolved oxygen concentration (Fig. 4), closely followed by oxygen production. Moreover, whereas at low kA_c values oxygen concentration appeared constant, it increased with larger kA_c values. This behaviour was previously observed in a single pass sealed RCER at oxygen concentrations below saturation [22].

5. Conclusion

Decrease in copper concentration followed the theoretical prediction in the presence of oxygen reduction in a multielement solution.

Current efficiency decreased with copper concentration. The oxygen reduction current efficiency increased, even when total current was reduced. At

copper concentrations below 1 ppm, current efficiency was nearly zero.

In a potentiostatically controlled undivided cell, the total current affected the anodic oxygen production which, in turn, influenced the dissolved oxygen concentration. The latter controlled the cathodic oxygen reduction current and thus affect the total current passing through the cell. Accordingly, a feedback loop was established for such a cell.

At rotation speeds over $100\,\mathrm{rad\,s^{-1}}$, this feedback loop resulted in higher oxygen reduction currents than theoretically predicted. The limiting current was proportional to the rotation speed ($I_l \propto \omega$) instead of following the semiempirical correlation ($I_l \propto \omega^{0.7}$). An increased rotation speed favours a greater oxygen reduction current efficiency, since the copper limiting current was found to always follow the semiempirical correlation.

For any given initial copper concentration, a lower rotation speed resulted in a higher time averaged current efficiency, but it took a long time to decrease copper concentration. Inversely, higher rotational speeds rapidly decreased the copper concentration at the expense of a lower time averaged current efficiency.

Acknowledgements

We are grateful to Environeau Inc. for the financial support given to produce this manuscript. Thanks are also extended to Louise Noreau for the chemical analysis and Andrea Corwin for grammatical corrections.

References

[1] D. G. Feasby, M. Blanchette, G. Tremblay and L. L. Sirois, *in* 'Second International Conference on Abatement of Acidic Drainage', vol. 1, Canada Center for Mineral and Energy Technology, Energy, Mines and Resources Canada, Ottawa (1991) p. 1.

[2] F. Ramade, 'Précis d'Écotoxicologie', Masson, Paris (1992).

[3] F. M. D'Itri, *in* 'Sediments: Chemistry and Toxicity of In-Place Pollutants', Lewis Publishers, Boston (1990) p. 163.

[4] C. Payette, W. W. Lam, C. W. Angle and R. J. Mikula, *in* 'Second International Conference on Abatement of Acidic Drainage', vol. 2, Canada Center for Mineral and Energy Technology, Energy, Mines and Resources Canada, Ottawa (1991) p. 15.

[5] M. Bergeron, R. Boisvert, S. Chevé, J. Cyr, D. Germain, M. Piotte, N. Massé, K. Oravec and N. Tassé, 'Restauration et Revalorisation de Parcs de Résidus Miniers', PMC-II project, report number 1, INRS-Géoressources, Ste-Foy, Québec (1992).

[6] PMC-II team, 'Restauration et Revalorisation de Parcs de Résidus Miniers, PMC-II project, report number 2, INRS-Géoressources, Ste-Foy, Québec (1993).

[7] INRS-Géoressources, 'Restauration et Revalorisation de Parcs de Résidus Miniers', PMC-II project, final report, INRS-Géoressources, Ste-Foy, Québec (1993).

[8] J. St-Pierre, N. Massé, É. Fréchette and M. Bergeron, 'Zinc Removal from Dilute Solutions using a Rotating Cylinder Electrode Reactor', *J. Appl. Electrochem.*, submitted.

[9] 'CRC Handbook of Chemistry and Physics', 65th edn, CRC Press, Boca Raton, Florida (1984).

[10] P. Strickland and F. Lawson, *Australas. Inst. Min. Metall. Proc.* **237** (1971) 71.

[11] G. Johansson, *Talanta* **12** (1965) 163.

[12] L. E. Vaaler, *J. Electrochem. Soc.* **125** (1978) 204.

[13] D. R. Gabe and F. C. Walsh, *in* 'The Reinhardt Schuhmann International Symposium on Innovative Technology and Reactor Design in Extractive Metallurgy' (edited by D. R. Gaskell, J. P. Hager, J. E. Hoffman and P. J. Mackey), The Metallurgical Society of AIME, Warrendale, PA (1986) p. 775.

[14] F. C. Walsh and D. R. Gabe, *Surf. Technol.* **12** (1981) 25.

[15] T. Takahashi, M. I. Ishmail and T. Z. Fahidy, *Electrochim. Acta* **26** (1981) 1727.

[16] D. R. Gabe, *J. Appl. Electrochem.* **4** (1974) 91.

[17] D. R. Gabe and F. C. Walsh, *ibid.* **13** (1983) 3.

[18] N. A. Gardner and F. C. Walsh, *in* 'Electrochemical Cell Design' (edited by R. E. White), Plenum Press, New York (1984) p. 225.

[19] F. C. Walsh, *in* 'Electrochemistry for a Cleaner Environment' (edited by J. D. Genders and N. L. Weinberg), Electrosynthesis Company Incorporated, East Amherst, New York (1992) p. 101.

[20] Z. A. Foroulis and H. H. Uhlig, *J. Electrochem. Soc.* **111** (1964) 13.

[21] I. Cornet and R. Kappesser, *Trans. Inst. Chem. Eng.* **47** (1969) T194.

[22] J. St-Pierre, N. Massé and M. Bergeron, *Electrochim. Acta* **39** (1994) 2705.

[23] J. St-Pierre, N. Massé and M. Bergeron, 'Dissolved Oxygen Concentration in a Divided Rotating Cylinder Electrode Reactor', *Electrochim. Acta*, accepted.